

# Oscillations of rotating magnetised neutron stars with purely toroidal magnetic fields

S. K. Lander<sup>\*</sup>, D. I. Jones<sup>†</sup> and A. Passamonti

*University of Southampton, Southampton, U. K.*

20 December 2009

## ABSTRACT

We investigate the oscillation spectrum of rotating Newtonian neutron stars endowed with purely toroidal magnetic fields, using a time evolution code to evolve linear perturbations in the Cowling approximation. The background star is generated by numerically solving the MHD equilibrium equations and may be nonspherical by virtue of both rotation and magnetic effects; hence our perturbations and background are fully consistent. Whilst the background field is purely toroidal, the perturbed field is mixed poloidal-toroidal. From Fourier analysis of the perturbations we are able to identify a number of magnetically-restored Alfvén (or  $a$ -) modes. We show that in a rotating star pure inertial and  $a$ -modes are replaced by hybrid magneto-inertial modes, which reduce to  $a$ -modes in the nonrotating limit and inertial modes in the nonmagnetic limit. We show that the  $r$ -mode instability is suppressed by magnetic fields in sufficiently slowly rotating stars. In addition, we determine magnetic frequency shifts in the  $f$ -mode. We discuss the astrophysical relevance of our results, in particular for magnetar oscillations.

**Key words:** MHD — stars: magnetic fields — stars: neutron — stars: oscillations — stars: rotation

## 1 INTRODUCTION

The identification of Soft Gamma Repeaters (SGRs) and Anomalous X-ray Pulsars (AXPs) as magnetars has reignited interest in the role played by magnetic fields in stellar dynamics. A class of neutron star (NS) with surface fields of  $\sim 10^{15}$  gauss, magnetars are the most highly magnetised stars yet observed. The SGRs are of special interest since in addition to their regular gamma-ray flares, they are also susceptible to occasional giant flares over three orders of magnitude more energetic than the regular flares. In the tails of these flares, high-frequency quasi-periodic oscillations (QPOs) have been observed (Israel et al. 2005; Watts & Strohmayer 2007) — these may be the first direct detections of neutron star oscillations. These QPOs should provide a valuable probe of the physics of the NS interior, but this requires an understanding of stellar oscillations in the presence of a strong magnetic field.

Neutron stars are not the only stars where magnetic effects may be important. The influence of a star’s magnetic field on its oscillation spectrum can be gauged from the ratio of its magnetic energy to the gravitational binding energy,  $M/|W|$ ; this suggests three classes of star where one should take account of the star’s magnetic field: in addition to NSs, there are also the rapidly-oscillating type-A peculiar (roAp) stars and magnetic white dwarfs (MWDs).

The earliest studies of magnetic star oscillations were driven by the discovery of  $\sim 10^4$  gauss fields — relatively strong for a main-sequence star — in some Ap stars (Chandrasekhar & Limber 1954; Ledoux & Simon 1957). Later, some of these stars were found to be oscillating at high frequency — the roAp stars — motivating a number of studies of magnetic effects on high-frequency  $p$ -modes (Unno et al. 1989; Dziembowski & Goode 1996; Rincon & Rieutord 2003). In addition to roAp stars, some white dwarfs have strong ( $\sim 10^9$  gauss) magnetic fields; these have shown no evidence of pulsation, perhaps due to magnetic suppression of the  $g$ -modes observed in weaker-field white dwarfs (Wickramasinghe & Ferrario 2000). Finally, the

<sup>\*</sup> skl@soton.ac.uk

<sup>†</sup> d.i.jones@soton.ac.uk

internal dynamics of neutron stars will be considerably affected by rotation as well as their strong magnetic fields, leading to interest in magnetic  $r$ -modes (Morsink & Rezzani 2002).

Many publications to date have reported on analytic studies of magnetic stellar oscillations, necessitating considerable simplifications to the problem: typically the model used is an incompressible star with a force-free background magnetic field. Some modern work on the problem has been inspired by the observation of magnetar QPOs, and this has tended to be numerical (Sotani et al. 2008; Sotani & Kokkotas 2009; Cerdá-Durán et al. 2009), with the advantages that more sophisticated physics can be modelled (for example, compressible and relativistic stars).

This paper is an investigation of the mode spectrum of magnetic stars through time evolution of the perturbed MHD equations. Here we consider only purely toroidal background fields, but in future we intend to investigate purely poloidal and mixed field stars too. We begin by perturbing the full system of equations to yield a set of equations for the background and another set for the perturbations. We improve on previous work on magnetic oscillations by solving the background equations in a self-consistent manner, so that the star is in exact equilibrium (up to some small numerical error), rather than simply using spherically symmetric density profiles and analytic results for the magnetic field configurations. We next discuss details of our time-evolution code and test its accuracy. After this, we present results for oscillations of stars with magnetic fields and rotation. Finally, we interpret these in the light of observed magnetic star oscillations and compare them with previous work on this subject.

## 2 BACKGROUND AND PERTURBATION EQUATIONS

We model a neutron star as a self-gravitating, rotating, magnetised polytropic fluid with perfect conductivity. The system is then governed by the equations of ideal magnetohydrodynamics (MHD):

$$\rho \left( \frac{\partial \mathbf{v}}{\partial t} + (\mathbf{v} \cdot \nabla) \mathbf{v} + 2\boldsymbol{\Omega} \times \mathbf{v} \right) = -\nabla P - \rho \nabla \Phi - \rho \boldsymbol{\Omega} \times (\boldsymbol{\Omega} \times \mathbf{r}) + \frac{1}{4\pi} (\nabla \times \mathbf{B}) \times \mathbf{B}, \quad (1)$$

$$\nabla^2 \Phi = 4\pi G \rho, \quad (2)$$

$$\frac{\partial \rho}{\partial t} = -\nabla \cdot (\rho \mathbf{v}), \quad (3)$$

$$\frac{\partial \mathbf{B}}{\partial t} = \nabla \times (\mathbf{v} \times \mathbf{B}), \quad (4)$$

$$P = k \rho^\gamma, \quad (5)$$

together with the solenoidal constraint  $\nabla \cdot \mathbf{B} = 0$  on the magnetic field. Here  $\mathbf{v}$  denotes the part of the fluid's velocity field which is not rigid rotation  $\boldsymbol{\Omega}$ ; all other symbols have their usual meanings. Throughout this paper we work with  $\gamma = 2$  polytropes exclusively, as a simple approximation to a neutron star equation of state. We consider linear Eulerian perturbations of this system by making the standard ansatz that each physical quantity has a zeroth-order background piece and a first-order perturbed piece; e.g. the density is written as  $\rho = \rho_0 + \delta\rho$ .

We assume that our background star is stationary and rigidly rotating, so that  $\boldsymbol{\Omega}$  is zeroth-order and  $\mathbf{v}$  first-order. Equations (3) and (4) become trivial and we are left with

$$0 = -\nabla P_0 - \rho_0 \nabla \Phi_0 - \rho_0 \boldsymbol{\Omega} \times (\boldsymbol{\Omega} \times \mathbf{r}) + \frac{1}{4\pi} (\nabla \times \mathbf{B}_0) \times \mathbf{B}_0, \quad (6)$$

$$\nabla^2 \Phi_0 = 4\pi G \rho_0, \quad (7)$$

$$P_0 = k \rho_0^\gamma. \quad (8)$$

Making the additional assumption of axisymmetry one may show that this system of equations splits into two cases: one where the magnetic field is purely toroidal and a second mixed-field case (with pure-poloidal fields as a limiting case). Details of the solution of these equations are given in Lander & Jones (2009); we use the code described therein to generate the background configurations used here. Here we merely note that our background configurations are fully self-consistent, with rotation, magnetic fields and fluid effects in equilibrium. In contrast to other work on magnetic oscillations, our background star need not be spherical, but may be distorted by rotational or magnetic effects, or a combination thereof.

For the perturbation equations, we work in the rotating frame of the background and write our equations in terms of the perturbed density  $\delta\rho$ , the mass flux  $\mathbf{f} = \rho_0 \mathbf{v}$  and a magnetic variable  $\boldsymbol{\beta} = \rho_0 \delta \mathbf{B}$ . We additionally make the Cowling approximation — neglecting the perturbed gravitational force — to avoid the computational expense of solving the perturbed Poisson equation. Our perturbations are then governed by seven equations:

$$\rho_0 \frac{\partial \mathbf{f}}{\partial t} = -\gamma P_0 \nabla \delta\rho - 2\boldsymbol{\Omega} \times \mathbf{f} + \left( \frac{(2-\gamma)\gamma P_0}{\rho_0} \nabla \rho_0 - \frac{1}{4\pi} (\nabla \times \mathbf{B}_0) \times \mathbf{B}_0 \right) \delta\rho + \frac{1}{4\pi} (\nabla \times \mathbf{B}_0) \times \boldsymbol{\beta} + \frac{1}{4\pi} (\nabla \times \boldsymbol{\beta}) \times \mathbf{B}_0 - \frac{1}{4\pi \rho_0} (\nabla \rho_0 \times \boldsymbol{\beta}) \times \mathbf{B}_0 \quad (9)$$

$$\frac{\partial \delta \rho}{\partial t} = -\nabla \cdot \mathbf{f}, \quad (10)$$

$$\frac{\partial \boldsymbol{\beta}}{\partial t} = \nabla \times (\mathbf{f} \times \mathbf{B}_0) - \frac{\nabla \rho_0}{\rho_0} \times (\mathbf{f} \times \mathbf{B}_0). \quad (11)$$

If we rewrite these equations in terms of  $\delta P = \frac{\gamma P_0}{\rho_0} \delta \rho$  and set the magnetic field to zero they reduce to the perturbation equations of Jones et al. (2002).

We next decompose each perturbed quantity in the azimuthal angle  $\phi$ ; for example  $\delta \rho$  becomes:

$$\delta \rho(t, r, \theta, \phi) = \sum_{m=0}^{\infty} \delta \rho_m^+(t, r, \theta) \cos m\phi + \delta \rho_m^-(t, r, \theta) \sin m\phi. \quad (12)$$

This reduces our problem from a 3D to a 2D one, at the expense of doubling the number of equations: we now have evolution equations in fourteen variables:  $f_r^\pm, f_\theta^\pm, f_\phi^\pm, \delta \rho^\pm, \beta_r^\pm, \beta_\theta^\pm, \beta_\phi^\pm$  for some value of  $m$  to be specified at the start of the evolution.

## 2.1 Boundary conditions

Rotational and magnetic forces will serve to distort the star's density distribution away from spherical symmetry and hence complicate the treatment of perturbations at the stellar surface. To avoid these complications we replace the radial coordinate  $r$  with one fitted to isopycnic surfaces,  $x = x(r, \theta)$ ; even a nonspherical surface will be defined by one value  $x \equiv R$ . With the background density being a function of  $x$  alone, we have  $\rho_0(x=R) = 0$  and hence

$$\mathbf{f}(x=R) = \boldsymbol{\beta}(x=R) = \mathbf{0}. \quad (13)$$

Finally, the Lagrangian pressure perturbation  $\Delta P$  is zero at the surface by definition. Relating this to the Eulerian perturbation we have

$$\delta P + \boldsymbol{\xi} \cdot \nabla P_0 = 0 \quad \text{at the surface.} \quad (14)$$

Using (6), we see that  $\nabla P_0$  may be written as two terms proportional to  $\rho_0$  and a term involving the magnetic current  $\nabla \times \mathbf{B}/4\pi$ . Both density and current are zero at the stellar surface and so  $\nabla P_0$  must also vanish there. This yields our last surface boundary condition:

$$\delta P(x=R) = 0. \quad (15)$$

Our boundary conditions allow us to evolve the interior magnetic field perturbations of our star, but not oscillations of the exterior. By contrast, one would expect magnetic perturbations in a physical neutron star to reach the surface and produce electromagnetic radiation extending through the exterior. Whilst our treatment of the surface does not account for this, we believe that it is the most that can be done using the equations of perfect MHD: in an infinitely-conducting polytropic star, a magnetic field that extends to the surface has a corresponding Alfvén speed  $c_A \equiv \sqrt{B^2/4\pi\rho}$  which becomes superluminal as  $\rho \rightarrow 0$ , and infinite when  $\rho = 0$  (i.e. the stellar surface and exterior). Dealing with the surface and exterior thus requires extra physics: a stellar model more sophisticated than a polytropic fluid with perfectly electrical conductivity. One could employ a low-density numerical atmosphere for the exterior, or assume that the field is confined or matches to some simplified crust — but these are merely numerical conveniences rather than good models of actual NS physics. In reality, perfect MHD ceases to be a good approximation close to the surface of a NS, where resistive effects become important and the full equations of electromagnetism should be used. The stellar surface is not fluid but an elastic crust; and the exterior will have a magnetosphere region rather than a dilute, uniform ‘atmosphere’.

Needless to say, a credible model star which included all these effects would give an oscillation spectrum closer to that of a real neutron star than the one we study here. In lieu of such a model, however, we treat oscillations over the fluid, highly-conductive interior of the star only. With magnetic fields being strongest here and  $\sim 99\%$  of the NS's mass consisting of a fluid interior, we anticipate that dynamics in this region would dominate the star's oscillation spectrum; and hence that our treatment is a reasonable first attempt to understand oscillations in real NSs.

Next we look at the conditions at the centre of the star. Since we deal with  $m > 0$  perturbations in this study, we should enforce a zero-displacement condition:

$$\delta P(x=0) = 0, \quad \mathbf{f}(x=0) = \boldsymbol{\beta}(x=0) = \mathbf{0}. \quad (16)$$

In general, a parity analysis of the perturbation equations of a fluid star shows that the variables may be classed according to their equatorial symmetry — either odd (the perturbation is zero along the equator) or even (its theta-derivative is zero). This division of the perturbations allows us to reduce our numerical domain to just one 2D quadrant and enforce the perturbation symmetry at the equator as another set of boundary conditions.

Analysing the perturbation equations for the (unmagnetised) rotating fluid problem, one finds that the perturbation variables may be divided into the two symmetry classes  $\{f_r^\pm, f_\phi^\pm, \delta \rho^\pm\}$  and  $\{f_\theta^\pm\}$ . In the case of a background star with a pure poloidal field these classes are augmented by magnetic variables, viz.  $\{f_r^\pm, f_\phi^\pm, \delta \rho^\pm, \beta_\theta^\pm\}$ ,  $\{f_\theta^\pm, \beta_r^\pm, \beta_\phi^\pm\}$ . Note that

although the background field is pure-poloidal, the perturbed field will still be mixed poloidal-toroidal. For a pure-toroidal background the magnetic perturbations are again mixed, but they fall into *different* symmetry classes from perturbations of a pure-poloidal star:  $\{f_r^\pm, f_\phi^\pm, \delta\rho^\pm, \beta_r^\pm, \beta_\phi^\pm\}$  and  $\{f_\theta^\pm, \beta_\theta^\pm\}$ . It follows that whilst we may separately treat perturbations on either a pure-poloidal or pure-toroidal background, the perturbations of a mixed-field background will have no definite equatorial symmetry. Investigating this latter group of perturbations requires an extended numerical domain consisting of an upper and lower quadrant. For this paper we concentrate only on oscillations of stars with purely toroidal background fields, postponing the pure-poloidal and mixed-field cases to future work.

### 3 NUMERICS

As described above, our numerical domain is one 2D quadrant of a circle, with  $x \in [0, 1]$  and  $\theta \in [0, \pi/2]$ ; by symmetry and through a  $\phi$ -decomposition this domain is sufficient to investigate behaviour over the whole 3D, potentially nonspherical, star. Upon decomposing in  $\phi$ , equations (9), (10) and (11) become a system of fourteen perturbation equations, which we evolve using a MacCormack predictor-corrector algorithm.

Our code is an extended version of the one described in Passamonti et al. (2009), where the authors demonstrated its accuracy and long-term stability for barotropic and stratified stars, in the nonmagnetic case. As in their work, we employ a fourth-order Kreiss-Oliger dissipation; this is an extra term added to the equations to damp spurious higher-order oscillations, i.e. those generated by the code's finite differencing. The magnitude of this term is resolution-dependent, so that it vanishes in the infinite-resolution continuum limit.

In addition to this dissipation, two further tricks are required to ensure stability and accuracy of magnetic evolutions. To stabilise the numerical evolution of the magnetic field, we first note that if the electrical resistivity  $\eta$  is non-zero, the induction equation gains an extra term:

$$\frac{\partial \mathbf{B}}{\partial t} = \nabla \times (\mathbf{v} \times \mathbf{B}) - \eta \nabla \times (\nabla \times \mathbf{B}). \quad (17)$$

By including this second term (at a small magnitude) we are able to suppress instabilities which arise from evolving the magnetic field. As for the Kreiss-Oliger dissipation, this artificial resistivity is added in a resolution-dependent manner, so it reduces to the correct (i.e. physical) continuum limit. We find that a very small value of  $\eta$  is sufficient to improve long-term stability, but has negligible physical effect on our evolutions, since it acts over a far longer timescale than any others in our problem.

#### 3.1 Divergence cleaning

Finally, for the long-term accuracy of the code we need to ensure that the perturbed magnetic field remains solenoidal. This is guaranteed in the continuum limit, since the divergence of the induction equation is

$$\frac{\partial(\nabla \cdot \mathbf{B})}{\partial t} = \nabla \cdot \nabla \times (\mathbf{v} \times \mathbf{B}) \equiv 0, \quad (18)$$

but in practice numerical error will be introduced from the finite grid resolution. It is important to ‘clean’ the field of this class of numerical error, since it has been shown that a numerically-generated monopolar field gives rise to a spurious extra force (Brackbill & Barnes 1980).

There are various approaches to divergence cleaning for numerical schemes. A review of these may be found in Dedner et al. (2002), where in addition a new constrained formulation of MHD is proposed, where the condition  $\nabla \cdot \mathbf{B} = 0$  is coupled to the induction equation through an auxiliary function; we repeat their argument below.

In the continuum limit the induction equation states that the vector  $\partial_t \mathbf{B}$  has a divergence-free part only, whereas a general vector can be decomposed into curl-free and divergence-free parts. Our discretised induction equation will no longer preserve this divergence-free aspect exactly and accordingly we add a curl-free term  $-\nabla\psi$  to the RHS, with  $\psi$  being some unknown function. We then couple our augmented induction equation to a relation for  $\psi$ :

$$\partial_t \mathbf{B} = \nabla \times (\mathbf{v} \times \mathbf{B}) - \nabla\psi \quad (19)$$

$$\mathcal{D}(\psi) = -\nabla \cdot \mathbf{B} \quad (20)$$

where  $\mathcal{D}$  is some linear differential operator. The Euler equation and the equation of mass conservation are unaffected. We now take the divergence of the first relation and the time derivative of the second:

$$\partial_t(\nabla \cdot \mathbf{B}) = -\nabla^2 \psi \quad (21)$$

$$\partial_t \mathcal{D}(\psi) = -\partial_t(\nabla \cdot \mathbf{B}) \quad (22)$$

which we combine to see that

$$\partial_t \mathcal{D}(\psi) = \nabla^2 \psi. \quad (23)$$

The choice of  $\mathcal{D}$  determines the way in which divergence errors are removed. The three basic types of cleaning are elliptic, parabolic and hyperbolic — so named because they entail solving a heat equation, wave equation or Poisson equation, respectively. Dedner et al. (2002) pioneer a mixed hyperbolic-parabolic approach, which they find to be superior to the simpler divergence-cleaning methods since it allows for errors to be propagated out of the star (hyperbolic cleaning) whilst simultaneously being damped (parabolic cleaning). The third method, elliptic cleaning, has the serious disadvantage that it requires the repeated solution of the (computationally expensive) Poisson equation; the mixed-hyperbolic scheme only adds the modest expense of having to evolve one more quantity — the function  $\psi$ .

Hyperbolic-parabolic divergence cleaning involves defining  $\mathcal{D}$  by

$$\mathcal{D}(\psi) = \frac{1}{c_h^2} \partial_t \psi + \frac{1}{c_p^2} \psi, \quad (24)$$

which leads to a telegraph (damped-wave) equation for  $\psi$ :

$$\partial_{tt} \psi = -\frac{c_h^2}{c_p^2} \partial_t \psi + c_h^2 \nabla^2 \psi. \quad (25)$$

Within the code, we implement this divergence-cleaning method through the evolution equation

$$\partial_t \psi = -\frac{c_h^2}{c_p^2} \psi - c_h^2 \nabla \cdot \mathbf{B} \quad (26)$$

together with our modified induction equation (19). Following Price & Monaghan (2005) we take  $c_h$ , the divergence-wave propagation speed, to be related to the sound  $c_s$  and Alfvén  $c_A$  speeds through the relation:

$$c_h = \sqrt{c_s^2 + c_A^2}. \quad (27)$$

The other coefficient is physically the inverse of the decay timescale  $\tau$ :

$$\frac{c_h^2}{c_p^2} = \frac{1}{\tau} \quad (28)$$

which Price & Monaghan (2005) argue is not universal, but rather should be modified to suit some lengthscale  $\lambda$  specific to the problem, i.e.

$$\frac{c_h^2}{c_p^2} = \frac{1}{\tau} = \frac{\alpha c_h}{\lambda}, \quad (29)$$

where  $\alpha$  is a dimensionless parameter. Using this result, we take  $\lambda$  to be the radial grid spacing  $\Delta r$  in our code. Finally then, our evolution equation for the function  $\psi$  is

$$\partial_t \psi = -\frac{\alpha \sqrt{c_s^2 + c_A^2}}{\Delta r} \psi - (c_s^2 + c_A^2) \nabla \cdot \mathbf{B}. \quad (30)$$

To close the system we need to give appropriate boundary conditions and initial data. For the latter we simply set  $\psi(t=0) = 0$  — this is reasonable because the initial data is divergence-free and so the variable  $\psi$ , associated with the monopole part of the magnetic field, should be zero initially.

For the boundary condition at the surface, we choose the Sommerfeld outgoing wave condition on  $\psi$ :

$$\partial_t \psi = -\sqrt{c_s^2 + c_A^2} (\partial_r \psi + \psi). \quad (31)$$

This result is for a spherical surface, but it still gives satisfactory cleaning in the case where the background star is spheroidal.

### 3.2 Testing the code

Since we already have confidence in the performance of the code in the nonmagnetic limit (see Passamonti et al. (2009) for details), we now test its accuracy and convergence properties with the inclusion of magnetic effects. To this end, we wish to monitor the divergence of the magnetic field and the total energy of the system (which should be conserved in the continuum limit). Since the background is stationary its total energy is automatically conserved; in addition the background field was constructed in a divergence-free manner (see Lander & Jones (2009)). Therefore it suffices to check conservation of the perturbed energy and the value of  $\nabla \cdot \delta \mathbf{B}$ .

To get a measure of the divergence of  $\delta \mathbf{B}$  over the *whole* star, rather than at individual points, we would like to evaluate  $\nabla \cdot \delta \mathbf{B}$  volume-integrated over the star. However, this quantity is first-order and so integrates to zero, so instead we define a ‘monopole energy’

$$\mathfrak{D} \equiv \frac{R^2}{8\pi} \int (\nabla \cdot \delta \mathbf{B})^2 dV \quad (32)$$

where  $R$  is the stellar radius; this energy should be insignificant in comparison with the perturbed magnetic energy  $\delta M$ . For each evolution used to generate results for this paper, the divergence of  $\delta \mathbf{B}$  was monitored through the dimensionless quantity

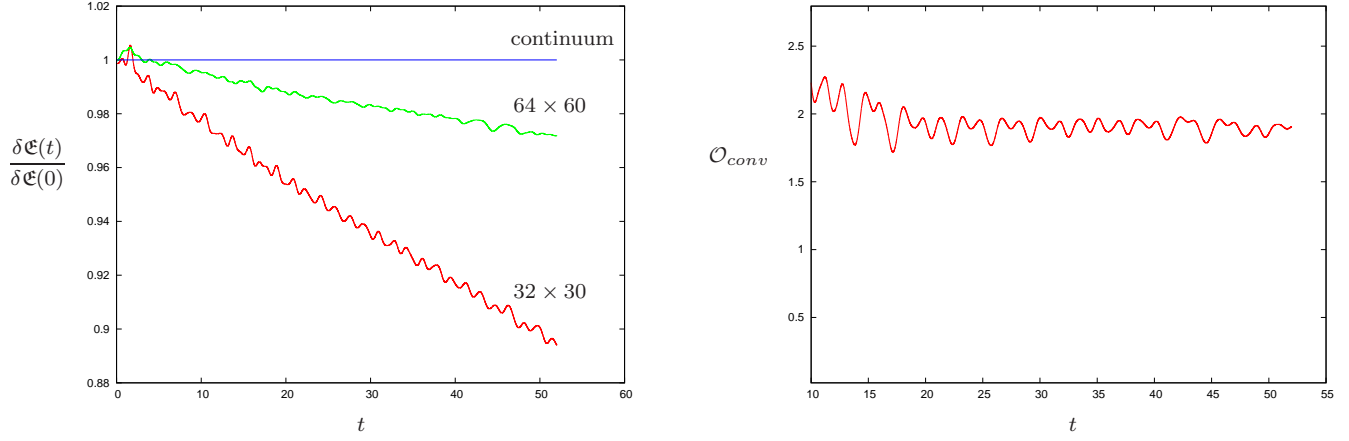


**Figure 1.** We determine the order of convergence of our code by evaluating the total perturbed energy  $\delta\mathfrak{E}$  over time; in the exact, continuum limit this quantity will not deviate from its initial value. The left-hand plot shows the deviation of  $\delta\mathfrak{E}$  from its initial value for  $(r, \theta)$  grids of  $32 \times 30$  and  $64 \times 60$  points. From these we confirm that the order of convergence  $\mathcal{O}_{conv}$  of the code is equal to 2, as intended (see right-hand plot).  $\mathcal{O}_{conv}$  is only plotted for  $t \geq 10$ , since at early times the numerical values of  $\delta\mathfrak{E}$  cross the continuum value, causing  $\mathcal{O}_{conv}$  to oscillate rapidly. The background configuration for these tests was a star with rotation rate  $\Omega/\sqrt{G\rho} = 0.238$  and with an average magnetic field strength  $\langle B \rangle = 2.87 \times 10^{16}$  G, evolved for 30  $f$ -mode oscillations.

$\mathfrak{D}/\delta M$ . Typically this quantity was found to be of the order  $\sim 0.01$ , rising to  $\sim 0.1$  in the case of very strong fields and rapid rotation rates.

Next we use conservation of (perturbed) energy to test the order of convergence of our code, using the fact that in the limit of infinite resolution energy should be exactly conserved. The total energy  $\delta\mathfrak{E}$  of the perturbations is given by

$$\delta\mathfrak{E} = \delta T + \delta W + \delta U + \delta M, \quad (33)$$

i.e. the sum of the perturbed kinetic  $T$ , gravitational  $W$ , internal  $U$  and magnetic  $M$  energies. Since we are making the Cowling approximation,  $\delta W = 0$  and we are left with

$$\delta\mathfrak{E} = \delta T + \delta U + \delta M = \int \left( \frac{1}{2} \rho_0 |\mathbf{v}|^2 + \frac{\gamma p_0}{2\rho_0^2} \delta\rho^2 + \frac{1}{8\pi} |\delta\mathbf{B}|^2 \right) dV. \quad (34)$$

This is in agreement with equation (C5) of Friedman & Schutz (1978) in the case of adiabatic perturbations within the Cowling approximation, but with an additional magnetic energy term. Note that all these terms are second-order quantities; the first-order energy vanishes for a background in equilibrium, and in our case each piece of it (for example the magnetic energy term proportional to  $\mathbf{B}_0 \cdot \delta\mathbf{B}$ ) is automatically zero by virtue of our  $\phi$ -decomposition.

To evaluate the convergence ratio, we monitor the evolution of the high-resolution energy  $\delta\mathfrak{E}_{64 \times 60}(t)$  and the medium-resolution energy  $\delta\mathfrak{E}_{32 \times 30}(t)$ , comparing these with the initial value of the energy  $\delta\mathfrak{E}(0)$ . In the continuum limit  $\delta\mathfrak{E}$  will have no time-dependence and will be equal to its initial value for all time. Hence we are able to use this exact result to define a convergence ratio

$$\mathcal{O}_{conv} = \frac{1}{\log 2} \log \left( \frac{\delta\mathfrak{E}_{32 \times 30}(t) - \delta\mathfrak{E}(0)}{\delta\mathfrak{E}_{64 \times 60}(t) - \delta\mathfrak{E}(0)} \right). \quad (35)$$

In figure 1 we evaluate  $\mathcal{O}_{conv}$  over time, confirming that the code is second-order convergent.

### 3.3 Nondimensionalising

Throughout the code we employ variables which have been made dimensionless through division by a suitable combination of powers of gravitational constant  $G$ , central density  $\rho_c$  and equatorial radius  $r_{eq}$ . For example, a dimensionless mode frequency  $\hat{\sigma}$  is related to the physical one  $\sigma$  (with units of  $\text{rad s}^{-1}$ ) through the relation  $\hat{\sigma} = \sigma/\sqrt{G\rho_c}$ ; the conversion is the same for rotational frequency  $\Omega$ . Since dimensionless frequencies of this form are common in oscillation mode literature we use these throughout this paper. Dimensionless magnetic field strengths, however, are less likely to be familiar and so we quote these in terms of gauss.

When we use dimensional quantities they are for a neutron star with canonical parameters: an equatorial radius of 10km (in the non-rotating, unmagnetised case) and a mass of  $1.4M_\odot$  (where  $M_\odot$  is solar mass). The relationship between dimensionless frequencies  $\hat{\sigma}$  (equivalently  $\hat{\Omega}$ ) and their physical counterparts is only weakly dependent on  $\Omega$  and  $\mathbf{B}$  — and hence is roughly linear, with

$$\sigma[\text{Hz}] \approx 1890\hat{\sigma}. \quad (36)$$

Finally, we note that in our dimensionless units, the Keplerian (break-up) velocity  $\Omega_K \approx 0.72$ . When we plot sequences of modes in rotating stars, we typically track the modes up to  $\Omega/\Omega_K \approx 0.95$ ; that is, rotation rates 95% of the break-up velocity.

## 4 RESULTS

### 4.1 Classes of oscillation mode

Using spherical polar coordinates, a general perturbation may be decomposed with respect to the basis  $(Y_{lm}\mathbf{e}_r, r\nabla Y_{lm}, \mathbf{e}_r \times \nabla Y_{lm})$ , where  $Y_{lm} = Y_{lm}(\theta, \phi)$  are the usual spherical harmonics. The first two of these terms transform by multiplication by  $(-1)^l$  under parity inversion  $\mathbf{r} \mapsto -\mathbf{r}$ , with the latter one transforming as  $(-1)^{l+1}$ . This enables us to classify modes based on their parity: those whose sign is given by  $(-1)^l$  under parity interchange as termed *polar* modes, whilst those transforming as  $(-1)^{l+1}$  are called *axial* modes. Hybrid modes, consisting of a sum of axial and polar pieces, are termed axial-led or polar-led based on whether the lowest- $l$  (i.e.  $l=m$ ) term of the mode is axial or polar, respectively.

For fixed  $m$ , Lockitch & Friedman (1999) found that inertial modes are not characterised by a single  $l$ , but have an angular dependence consisting of a sum of spherical harmonics  $Y_{lm}(\theta, \phi)$ . However, in all cases they found there was some threshold value  $l_0$ , such that the amplitude of  $Y_{lm}$  contributions for  $l > l_0$  was found to drop off rapidly. Following their work, we label modes using the notation  ${}^{l_0}_m a_k$ , where  $k$  distinguishes between different modes with the same  $l_0$ .

A non-rotating, unmagnetised fluid star has only one class of oscillation modes if the perturbations are assumed to have the same equation of state as the background star. These are the  $p$ -modes, whose restoring force is pressure fluctuations; the lowest-order  $p$ -mode (i.e. the one with a nodeless eigenfunction) in each series is termed the fundamental mode, or  $f$ -mode. The non-axisymmetric  $p$ -modes are degenerate in the absence of rotation and magnetic fields; each  $p$ -mode has the same frequency for fixed  $m$ . These modes are polar in nature.

With a rotating background star, a Coriolis force term enters the equations governing the perturbations, which removes the  $m$ -degeneracy in the  $p$ -modes. The Coriolis term is the restoring force for a new class of modes: the inertial modes, which we term  $i$ -modes. In general  $i$ -modes are mixed axial and polar even in the slow-rotation limit, but one class of them are purely axial in this limit: the  $r$ -modes. With the barotropic equation of state we employ here, the only  $r$ -modes which exist are those with  $l=m$ .

Finally, magnetic fields also induce a class of oscillation mode, restored by the Lorentz force. We term them the Alfvén modes, or  $a$ -modes. In addition to generating a new class of modes, the Lorentz force can lift degeneracies of nonradial oscillations, causing a splitting in mode frequencies (Cox 1980). The addition of the Lorentz force term in the Euler equation for the perturbations should produce shifts in the frequencies of the  $p, r$  and  $i$  modes from their unmagnetised values.

### 4.2 Initial data

Having performed a  $\phi$ -decomposition of our perturbation variables, we fix a value for the azimuthal index  $m$  for each evolution. However, since we have no restrictions on  $\theta$ -dependence, oscillations for a variety of  $l \geq m$  will typically be excited for arbitrary initial data — hence we are able to study several modes at once. The nature of these modes is then determined from analysis of their eigenfunctions, as well as by tracking them back to a regime where we already know their properties.

Whilst any initial data will excite a variety of modes, we choose different starting perturbations depending on whether we wish to investigate axial/axial-led or polar/polar-led modes. For polar modes we provide a density perturbation whose angular dependence is given by an ordinary spherical harmonic; for axial modes we use a ‘magnetic’ spherical harmonic-dependent velocity perturbation. In both cases the radial dependence is a Gaussian profile. More details about these choices may be found in Jones et al. (2002).

### 4.3 Mode spectrum of a non-rotating magnetised star

In this section we present results for nonrotating stars, since the mode spectrum is simpler, leaving rotating stars to the next section. We begin by investigating the new class of modes present with the addition of a magnetic field, the  $a$ -modes. Results are presented for both polar and axial  $a$ -modes.

Let us begin by considering where in the frequency spectrum these modes could be expected. Now, any mode frequency will be proportional to some characteristic wave speed. For fluid modes like the  $f$ -mode, the frequency should be proportional to the sound speed  $c_s$ ; similarly the  $a$ -mode frequencies should be proportional to the Alfvén speed  $c_A$ . Accordingly the ratio of frequencies should scale as

$$\frac{\sigma_f}{\sigma_a} \sim \left\langle \frac{c_s}{c_A} \right\rangle \quad (37)$$

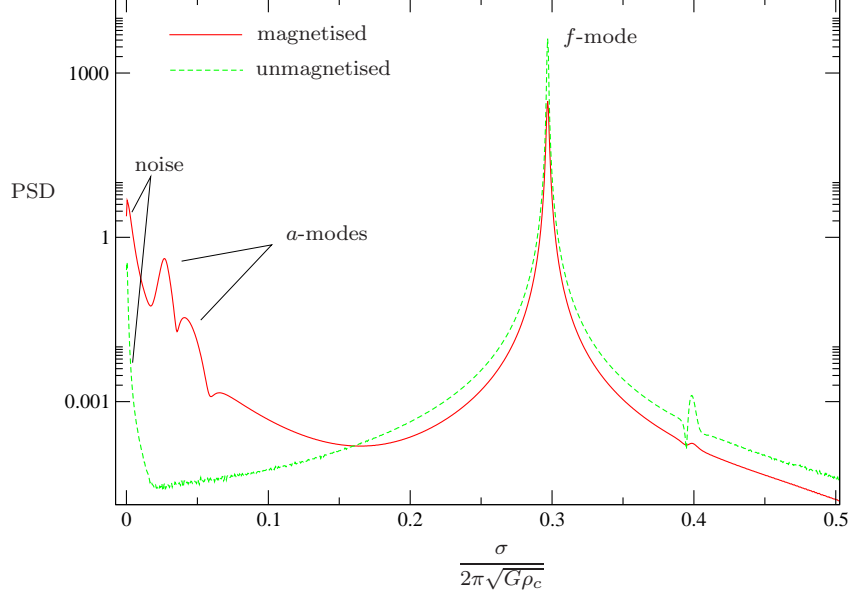


**Figure 2.** Typical FFT results for a pair of nonrotating stars, one magnetised and the other unmagnetised. We plot mode frequency  $\sigma$  (in a dimensionless form) against PSD, the power spectral density. We see that the  $f$ -mode frequencies are very close in both cases. With no Coriolis force there are no inertial modes, therefore any peaks at lower frequency than the  $f$ -mode must be either noise or Alfvén modes. We identify the lowest-frequency spike in the magnetic FFT as noise, since there is a corresponding unphysical peak in the nonmagnetic FFT. The following peaks in the magnetised-star FFT, however, have no analogue in the nonmagnetic FFT and so we identify these as Alfvén modes. The duration of the evolution was sufficient to resolve around 100 Alfvén oscillations.

where the angle brackets represent a volume average. Now

$$\frac{c_s}{c_A} = \sqrt{\frac{\gamma P}{\rho}} \bigg/ \sqrt{\frac{B^2}{4\pi\rho}} \quad (38)$$

and so

$$\left\langle \frac{c_s}{c_A} \right\rangle = \frac{2\sqrt{\pi\gamma\langle P \rangle}}{\langle B \rangle}. \quad (39)$$

We find from our background code that a nonrotating unmagnetised  $\gamma = 2$  polytrope with a mass of  $1.4M_\odot$  and radius  $R = 10$  km has a volume-averaged pressure  $\langle P \rangle$  of  $3.10 \times 10^{34}$  dyn cm $^{-2}$ . Using this value and  $\langle B \rangle = 10^{16}$  G to nondimensionalise, we find that

$$\frac{\sigma_f}{\sigma_a} \sim 90 \times \left( \frac{\langle P \rangle}{3.10 \times 10^{34} \text{ dyn cm}^{-2}} \right)^{1/2} \left( \frac{\langle B \rangle}{10^{16} \text{ G}} \right)^{-1}. \quad (40)$$

With the value of  $\langle P \rangle$  varying little with magnetic field strength, we assume that it is a constant and that  $\sigma_f/\sigma_a$  scales only with  $\langle B \rangle$ . It then follows that we should expect  $\sigma_a$  to be roughly 1/90 of  $\sigma_f$  for a  $10^{16}$  G field, but 1/9 of  $\sigma_f$  for a  $10^{17}$  G field. This part of the spectrum is dominated by inertial modes in the case of unmagnetised rotating stars, but in the absence of rotation we may be confident that any oscillations at lower frequency than the  $f$ -mode are associated with the magnetic field — see figure 2.

Now, with  $\sigma_a \propto \langle c_A \rangle$  and  $c_A = B/\sqrt{4\pi\rho}$ , it follows that  $\sigma_a \propto B$ , provided that magnetic changes to the density distribution are higher order (which should be true for all but very high fields — see Lander & Jones (2009)). To summarise,  $a$ -modes should scale linearly with field strength and appear as oscillations with lower frequency than the  $f$ -mode. With these expectations, we now turn to numerical results from our time-evolution code.

In figure 3 we track a number of Alfvén mode frequencies up to averaged-field strengths of order  $10^{17}$  gauss. For axial initial data and fixed  $m$  we find a single  $l=m$  mode, whilst polar initial data excites two  $l_0 = m+1$  modes for a given  $m$ . In all cases, we see that as expected there is a near-linear relationship between  $\sigma_a$  and  $\langle B \rangle$ . The identification of the  $a$ -modes is based on analysis of their eigenfunctions, using the numerical method of Stergioulas et al. (2004). The labelling used here anticipates the results of the next section, where we track these modes for increasing rotation rate.

At the start of this section we showed that the  $a$ -mode frequency should vary linearly with  $\langle B \rangle$ , and this appears to be

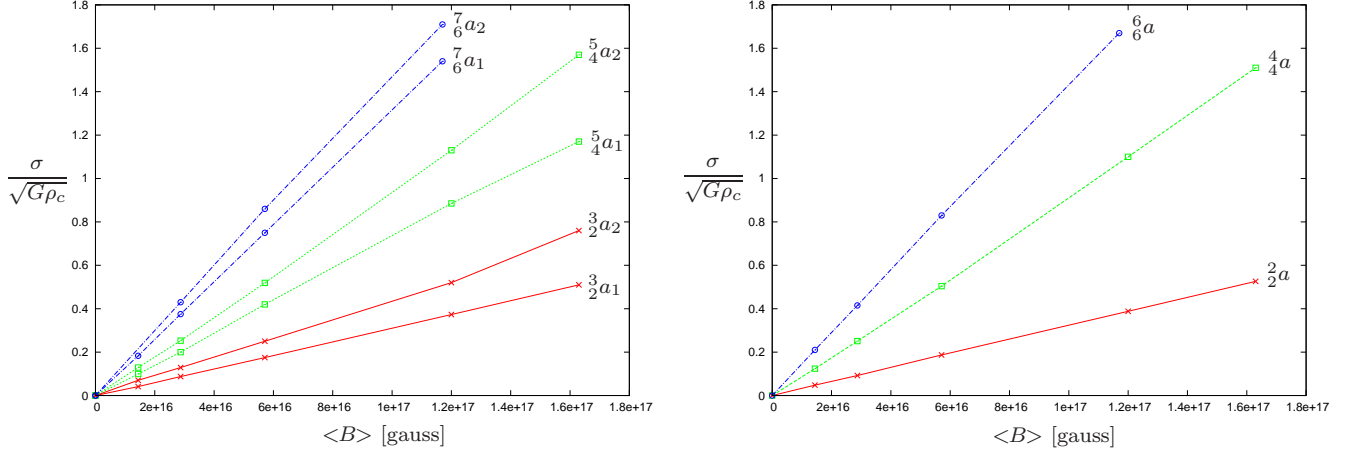


**Figure 3.** Polar  $l_0 = m + 1$  Alfvén modes (left) and axial  $l = m$  Alfvén modes (right), for  $m = 2, 4, 6$ . Tracking the modes to high field strength, we see that each mode frequency scales linearly with magnetic field strength, as anticipated. These results are for a nonrotating star.

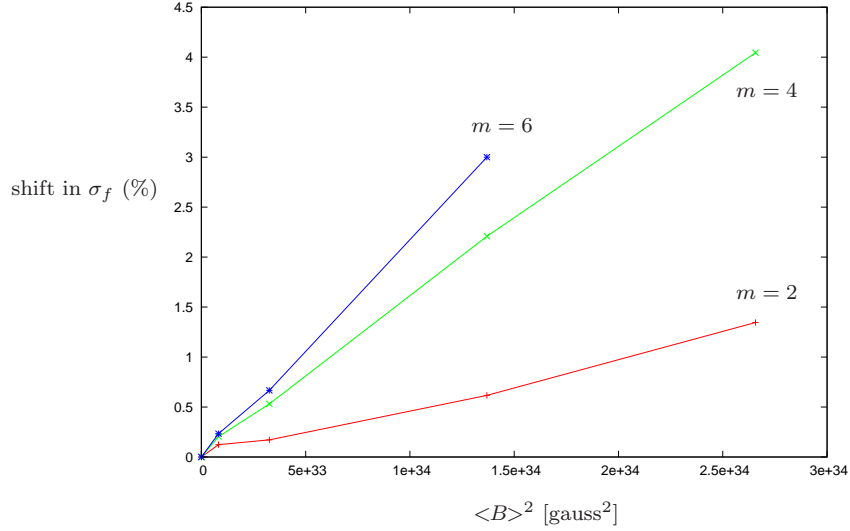


**Figure 4.** The shift in  $f$ -mode frequency due to magnetic effects (for nonrotating stars), for  $m = 2, 4, 6$ . On the  $y$ -axis we plot percentage increase in  $\sigma_f$  from its unmagnetised value; we see that this shift appears to depend quadratically on  $\langle B \rangle$ . The apparent deviation from this dependence, visible in the weakest-field results, is attributable to numerical errors in these very small frequency shifts.

borne out by our results. We now quantify this dependence and the deviation from it. By looking at the weak-field results from our code (where the relationship should be closest to linear), we determine the constants of proportionality in the relationship

$$\frac{l_0(\sigma_a)_k}{\sqrt{G\rho_c}} = l_0 c_k \left( \frac{\langle B \rangle}{10^{16} \text{ G}} \right), \quad (41)$$

finding that  $\frac{1}{2}c = 0.033$ ,  $\frac{3}{2}c_1 = 0.030$ ,  $\frac{3}{2}c_2 = 0.045$ ,  $\frac{4}{4}c = 0.086$ ,  $\frac{5}{4}c_1 = 0.069$ ,  $\frac{5}{4}c_2 = 0.090$ ,  $\frac{6}{6}c = 0.146$ ,  $\frac{7}{6}c_1 = 0.127$ ,  $\frac{7}{6}c_2 = 0.150$ . For all our results the linear relationship (41), with the numerically-established constants  $l_0 c_k$ , agrees to within 8% of the mode frequencies we have extracted from our evolutions — and in most cases the difference is less than 5%.

Finally in this section, we look at the shift in the frequency of the fundamental mode upon the addition of a magnetic field to the star. This mode is restored by perturbations in the fluid pressure  $P$  in the unmagnetised case, so we anticipate that in the magnetic problem the restoring force is perturbations of *total* (fluid plus magnetic) pressure,  $P + B^2/8\pi$ . The magnetic shift in  $\sigma_f$ , then, should be proportional to  $B^2$  — but since magnetic pressure is very modest in magnitude compared with fluid pressure, we expect the frequency shift to be small. For example, using our canonical model star, the magnetic pressure is  $\sim 1\%$  of the fluid pressure at  $10^{17}$  G. We confirm these expectations in figure 4. In all cases  $\sigma_f$  is increased by the inclusion of magnetic effects, but the shifts are only around a couple of percent even for  $\langle B \rangle \sim 10^{17}$ . The relative shift appears to be more pronounced for higher- $m$  oscillations.

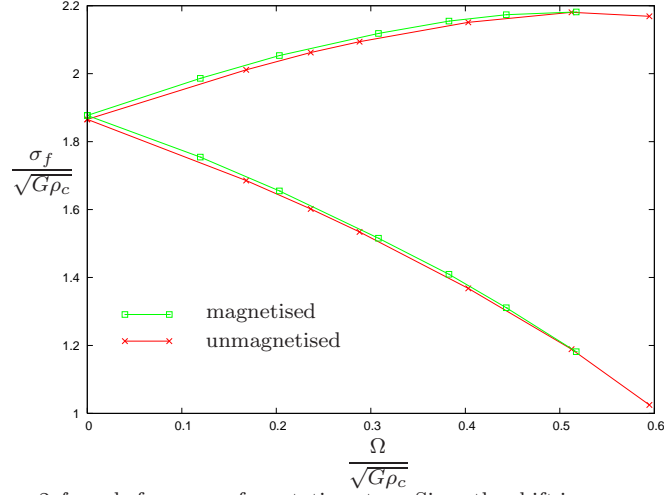


**Figure 5.** Magnetic shift of the  $m = 2$   $f$ -mode frequency for rotating stars. Since the shift is very small we take a very highly magnetised background star, with  $\langle B \rangle = 1.17 \times 10^{17}$  G for comparison with the nonmagnetic sequence of results. We find that as the rotation rate  $\Omega$  increases, magnetic effects become less significant.

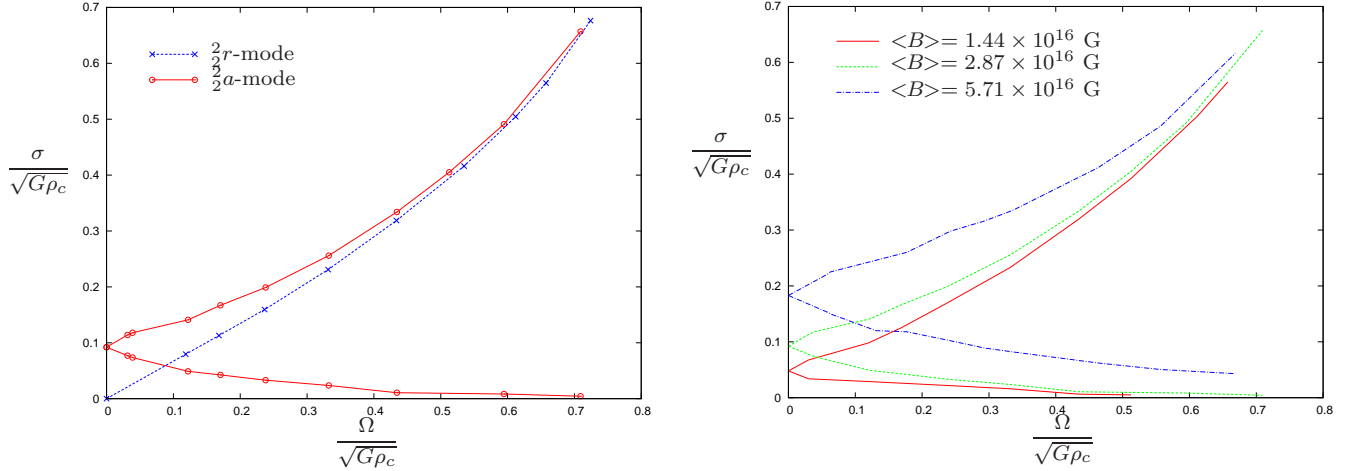


**Figure 6.** Illustrating the hybrid inertial-magnetic nature of modes in a rotating magnetised star. When  $\Omega = 0$  there is a pure  $l = m = 2$   $a$ -mode, which is split into co- and counter-rotating modes by the effect of rotation. The counter-rotating mode frequency approaches the nonmagnetic  $r$ -mode frequency as  $\Omega$  increases, while the corotating branch tends to zero frequency. The left-hand plot compares the  $\frac{3}{2}a$  mode with the  $r$ -mode, whilst the right-hand plot shows that the nature of the hybrid mode depends on the ratio  $M/T$ ; when  $\langle B \rangle$  is larger, the  $\frac{3}{2}a$ -mode frequency approaches the  $r$ -mode frequency more slowly. Modes are tracked up to  $\Omega \approx 0.7$  in dimensionless units, which is over 95% of the break-up velocity. The irregular parts of the curves may correspond to avoided crossings with other magneto-inertial modes.

#### 4.4 Mode spectrum of a rotating magnetised star

Armed with some idea of the mode spectrum of magnetised nonrotating stars, we next consider rotating magnetised configurations. The earliest studies of magnetic oscillations suggested that the significance of the magnetic field on the oscillation spectrum should be linked to the ratio  $M/|W|$ ; when additionally including rotational effects we would expect the relative significance of the two effects to be related to  $M/T$ .

We first consider magnetic shifts in the  $f$ -mode frequency for rotating stars. Rotation splits the  $f$ -mode into co- and counter-rotating modes; we expect the frequencies of both branches of the mode to shift with the addition of magnetic fields. At low rotation, the magnetic shift for each piece of the  $f$ -mode is comparable with the shift in the nonrotating case, but at higher rotation rates the shift becomes less significant — see figure 5. This bears out our expectation that the magnetic shift should scale with  $M/T$ .

We next turn to  $a$ -modes and  $r$ -modes of rotating magnetised stars. Based on our experience so far, we have expectations on how each mode should behave. We anticipate a rotational splitting of the  $a$ -modes into co- and counter-rotating pieces (as seen for the  $f$ -mode); in addition we expect to see some magnetic shift, scaling with  $M/T$ , in the  $r$ -mode.

We begin by tracking the axial  $\frac{3}{2}a$ -mode with increasing rotation, finding that as expected it undergoes rotational splitting

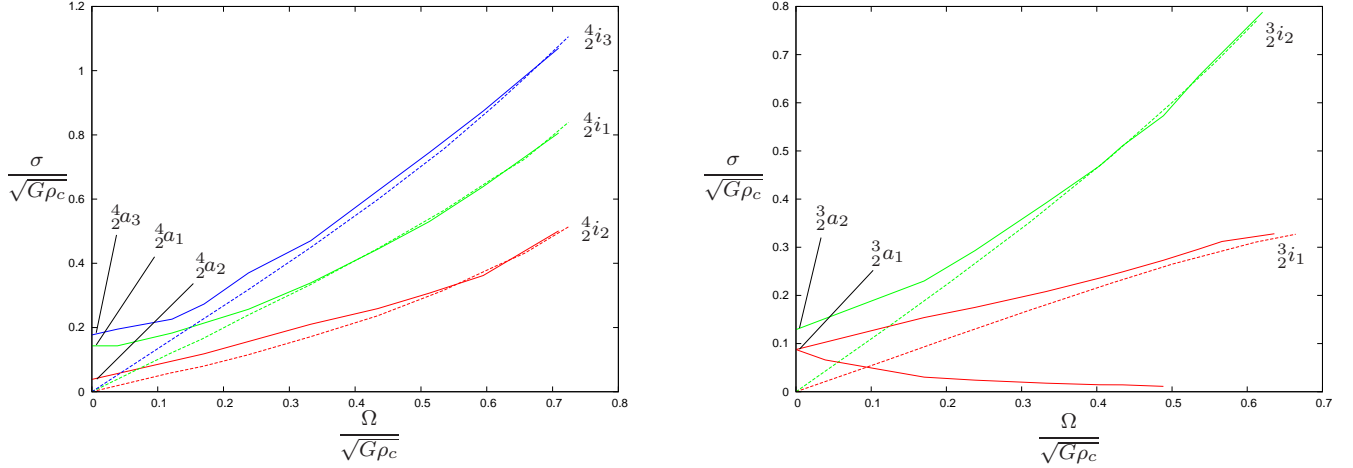


**Figure 7.** The  $m=2, l_0=3, 4$  hybrid magneto-inertial modes. Dashed lines represent the pure inertial ( $\langle B \rangle = 0$ ) modes, whilst solid lines show magneto-inertial modes, which reduce to pure Alfvén modes in the  $\Omega \rightarrow 0$  limit. The left-hand plot shows the  $l_0=4$  (axial) hybrid modes, whilst the right-hand plot shows  $l_0=3$  (polar) modes. In each case the upper-frequency branch of a hybrid mode is seen to meet a corresponding  $i$ -mode as  $M/T \rightarrow 0$ . For the  $\frac{3}{2}a_1$  mode, we were also able to track the lower-frequency branch, which appears to reduce to a zero-frequency mode in the  $M/T \rightarrow 0$  limit.

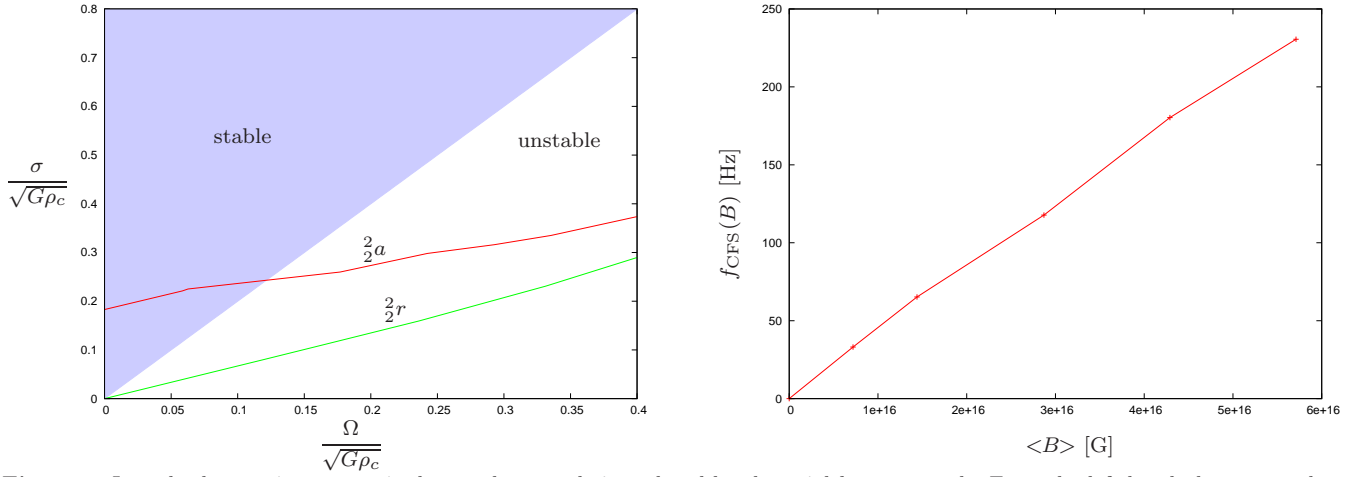


**Figure 8.** In a slowly-rotating magnetised star, the  $r$ -mode is replaced by the axial  $l=m$   $a$ -mode. From the left-hand plot we see that this mode is not subject to the CFS instability if  $\Omega$  is sufficiently small, but at some higher rotational frequency  $f_{\text{CFS}}$  (a function of the field strength  $B$ ) the  $a$ -mode crosses into the unstable regime. The right-hand plot shows the variation of  $f_{\text{CFS}}$  with average field strength  $\langle B \rangle$ .

(figure 6). The lower-frequency branch of this  $a$ -mode appears to tend to zero with increasing  $\Omega$  (or equivalently, as  $M/T \rightarrow 0$ ). The higher-frequency branch of the  $a$ -mode tends to the  $r$ -mode frequency as  $M/T \rightarrow 0$ . We confirm that the magnetic/inertial character of these hybrid modes depends on  $M/T$  by tracking the  $\frac{2}{2}a$ -mode for three different field strengths, finding that when  $\langle B \rangle$  is higher the hybrid-mode frequency approaches the  $r$ -mode frequency more slowly. The higher-frequency branch of the  $\frac{2}{2}a$  mode is counter-rotating and joins up with the  $r$ -mode, whilst the lower-frequency  $\frac{2}{2}a$  mode corotates with the star.

Having established that the pure  $\frac{2}{2}a$  mode and the pure  $r$ -mode are replaced by a hybrid magneto-inertial mode when both magnetic and rotational restoring forces are present, one would expect to find similar hybrid modes corresponding to other Alfvén/inertial modes; we confirm this expectation in figure 7. As before, rotation splits each  $a$ -mode into co- and counter-rotating branches. We are able to track the upper-frequency branches of both polar  $\frac{3}{2}a$ -modes to their inertial counterparts, and all three  $\frac{4}{2}a$ -modes to known inertial modes in the  $M/T \rightarrow 0$  limit. In addition, we are able to track the lower-frequency branch of the  $\frac{3}{2}a_1$  mode to high rotation rates; it appears to become a zero-frequency mode in the  $M/T \rightarrow 0$  limit, as for the lower  $\frac{2}{2}a$ -mode.

A number of modes are subject to instabilities driven by gravitational radiation emission, but in general only become unstable for sufficiently rapid rotation. However, the  $r$ -modes are unstable even in very slowly rotating stars, in the absence of viscosity (Andersson & Kokkotas 2001). We have already seen that magnetic fields significantly alter the behaviour of the  $r$ -mode for slow rotation, so we now consider the effect this has on their stability. For a counter-rotating mode with frequency

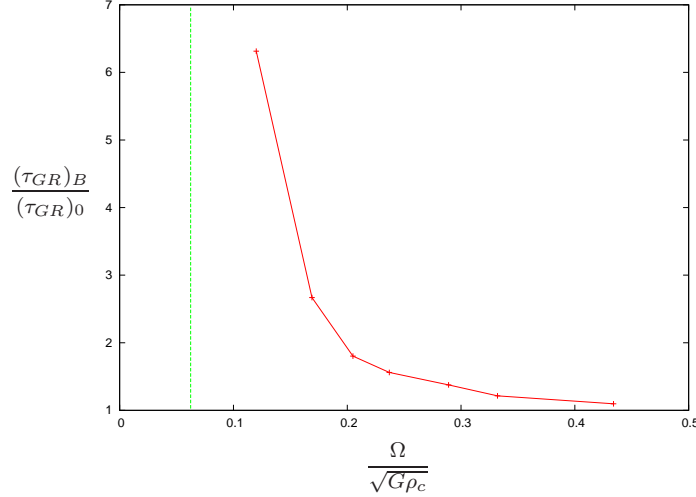


**Figure 9.** A magnetic field changes the growth time of the  $r$ -mode instability. Here we plot an approximation of the ratio of magnetised  $(\tau_{GR})_B$  to unmagnetised  $(\tau_{GR})_0$  growth timescales, against dimensionless rotation rate. The dashed vertical line shows where the ratio asymptotes (i.e. when the magnetised mode becomes stable). We see that in all cases the instability growth is slower with magnetic effects, but the effect becomes insignificant for rapid rotation. The magnetic timescales used were for a star with a field of  $2.87 \times 10^{16}$  G.

$\sigma$  (positive by convention) in the rotating frame, the instability criterion is

$$\sigma(\sigma - m\Omega) < 0. \quad (42)$$

It follows immediately that radiative instabilities are suppressed when  $\sigma > m\Omega$ . In the left-hand part of figure 8 we plot this threshold frequency, together with the nonmagnetic  $r$ -mode and the hybrid mode that replaces it in the magnetic case. It is clear that whilst the unmagnetised  $r$ -mode is always in the unstable regime, its magnetic equivalent (the hybrid of the  $r$ -mode and the axial  $l = m$   $a$ -mode) is stable for sufficiently low rotation rates. The maximum rotational frequency a star can have before its  $\frac{3}{2}r$  mode goes unstable is plotted on the right-hand side, as a function of the stellar magnetic field strength.

Even when magnetic fields are not strong enough to suppress the  $r$ -mode instability, they may slow down its growth. A full calculation of this effect is beyond the scope of this paper, but we may estimate it with some simplifying assumptions. The growth time  $\tau_{GR}$  of the  $r$ -mode instability due to gravitational radiation is given by

$$\frac{1}{\tau_{GR}} = -\frac{1}{2E} \frac{dE}{dt} \quad (43)$$

where  $E$  is the energy of the mode in the rotating frame. From this one can show that the growth time  $\tau_{GR}$  scales with the rotating-frame mode frequency  $\sigma$  in the following manner for an  $l = m$   $r$ -mode:

$$\frac{1}{\tau_{GR}} \sim \sigma(\sigma - l\Omega)^{2l+1} \quad (44)$$

— see Andersson & Kokkotas (2001) for details. Note that for  $l = m = 2$ , the growth time scales with the sixth power of  $\sigma$ .

We wish to estimate how the growth time for the  $\frac{3}{2}r$ -mode changes when magnetic effects are included. Since  $\tau_{GR}$  contains a factor of  $\sigma^6$ , we will assume that this term has the most significant variation when a magnetic field is added. Other terms in the expression of  $E$  and its derivative will be approximated as constant. Using the indices 0 and  $B$  to denote nonmagnetic and magnetic quantities (respectively), we then see that

$$\frac{(\tau_{GR})_B}{(\tau_{GR})_0} \approx \frac{\sigma_0(\sigma_0 - 2\Omega)^5}{\sigma_B(\sigma_B - 2\Omega)^5}. \quad (45)$$

In figure 9 we plot this dimensionless quantity as a function of the rotation rate, finding that a toroidal magnetic field does indeed slow down the instability's growth. The importance of the effect depends on the rotation rate: at twice the threshold frequency for stability of the magnetised  $r$ -mode (i.e. when the mode is unstable), its growth time is still a factor of  $\sim 6$  longer than in the nonmagnetic  $r$ -mode case; however, for very rapid rotation the difference in growth times is negligible.

## 5 DISCUSSION AND CONCLUSIONS

In this paper we have investigated oscillation modes of neutron stars with rotation and magnetic fields, specialising to the case of purely toroidal background fields; we intend to study purely poloidal and mixed-field geometries in future publications. Our numerical approach allows us to study oscillations of rapidly rotating and highly magnetised stars in a self-consistent manner. We first generate a stationary star in equilibrium to use as the background configuration; this star may have axisymmetric

distortions due to magnetic effects and rotation. We then time-evolve linear perturbations on this background star in order to study its modes of oscillation.

When a magnetic field is added to a star, the most obvious change to its oscillation spectrum is the presence of Alfvén ( $a$ -) modes, a class of stellar oscillation restored by the Lorentz force. These modes are purely magnetic in nature only for a nonrotating background star.

In a rotating magnetised star, we find that the pure  $a$ -modes of a nonrotating star (or equivalently, the purely inertial  $i$ -modes of an unmagnetised star) are replaced by hybrid magneto-inertial modes, whose character is governed by the ratio of the magnetic  $M$  and kinetic  $T$  energies, as discussed by Morsink & Rezanian (2002). Tracking a star at fixed magnetic field from  $\Omega = 0$  through increasing rotation rate, we see a rotational splitting of the  $a$ -modes into co- and counter-rotating modes. The higher-frequency branches of these modes approach known  $i$ -mode frequencies. In general the lower-frequency branches are harder to track, owing to the dense nature of the oscillation spectrum, but when we are able to identify them we find that they appear to become zero-frequency modes in the  $M/T \rightarrow 0$  limit.

The presence of these hybrid modes has parallels with other work. The evolutions of Passamonti et al. (2009) and Gaertig & Kokkotas (2009) found that when tracking  $g$ -modes (i.e. modes restored by composition gradients within the star) for increasingly rapid rotation, their frequencies approached known  $i$ -mode frequencies. One key difference between stratified and magnetised stars, however, is the behaviour of the  $r$ -mode in each case. Being purely axial in the slow-rotation limit, the  $r$ -modes are unaffected by composition gradients, whereas we have found that the presence of a magnetic field means that in the slow-rotation limit they become the axial  $l = m$   $a$ -mode.

Our work seems to be consistent with the analysis of Glampedakis & Andersson (2007), who found that magnetic fields could act to suppress instabilities driven by gravitational radiation (the CFS instability); and in particular, that purely poloidal or purely toroidal fields should always play a stabilising role in this case. Using  $\sigma$  to denote a mode frequency as measured in the rotating frame, it is known that modes satisfying the condition  $\sigma(\sigma - m\Omega) < 0$  are susceptible to these radiation-driven instabilities; in particular, this includes the  $r$ -mode. In the presence of a magnetic field we find that the  $r$ -mode is replaced by the  $l = m$  axial  $a$ -mode; for sufficiently slow rotation we have  $\sigma_a > m\Omega$  and hence the mode is CFS-stable. In the regime where the star is unstable, we use a simple estimate to suggest that the instability's growth will be slower in the presence of a magnetic field.

In addition to the hybrid magneto-inertial modes, there are also magnetic corrections to the  $f$ -mode frequency. These corrections are very modest ( $\sim 1\%$ ) even up to field strengths of the order  $10^{17}$  gauss. In addition, as for the magneto-inertial modes, the magnetic correction becomes less significant still as  $M/T \rightarrow 0$ . However, we note that the magnetic correction seems to increase between  $m = 2$  and  $m = 6$ , so although our approach limits us to low  $m$  one might expect more appreciable corrections to high- $m$   $f$ - and  $p$ -modes.

Although it would be premature to make a quantitative comparison between our results and observed magnetar QPOs, we note that there are certain similarities in the oscillation spectra. The QPOs observed from SGR 1806-20 include 26 and 30 Hz modes; these cannot be explained as overtones of crustal shear modes because the spacing is too small (they would need to be integer multiples for this). By contrast, it is easy to interpret these frequencies as global modes of a fluid star (i.e. the magnetar's interior), since we see modes at far smaller separation than integer multiples. For example, using our fitted relation (41) we see that the frequency ratio of the axial  ${}_2a$  and polar  ${}_3a_1$  modes is  $0.030/0.033 \approx 0.91$  — comparable with the observed ratio of  $26/30 \approx 0.87$ .

This paper adds to the picture of magnetic stellar oscillations built up by a number of other recent numerical studies. The work of Sotani et al. (2008) and Cerdá-Durán et al. (2009) investigated axial magnetar oscillations, modelling the star's magnetic field as dipolar (and hence purely poloidal). They found two localised families of QPOs, which they related to observed magnetar QPOs. Colaiuda et al. (2009) worked on a similar problem, but in the more general case of a mixed poloidal-toroidal background field. Their work complements other studies, but they are also able to identify a third family of QPOs in their model star. Finally, Sotani & Kokkotas (2009) find a set of polar oscillations of dipolar fields, agreeing with the work of Lee (2007) that a magnetar should have both axial and polar oscillations.

Many of these recent studies have analysed their results in the light of the suggestion that magnetic oscillations of a perfectly-conducting star form a continuum, rather than discrete modes. This was proposed by Levin (2007), revisiting earlier work by Goossens et al. (1985). Various numerical studies (Sotani et al. 2008; Cerdá-Durán et al. 2009; Colaiuda et al. 2009) have found results consistent with this proposal, in the case of axial oscillations of a dipole field. However, Sotani & Kokkotas (2009) suggest that *polar* oscillations of a dipolar-field star are discrete.

Since our background field is purely toroidal, we cannot make quantitative comparisons with work discussed in the last two paragraphs, since those studies assumed dipolar fields (or mixed poloidal-toroidal fields in the case of Colaiuda et al. (2009)). However, we do find broad similarities — in particular, our  $a$ -mode frequencies are of the order 100 Hz (for a field of  $\sim 10^{16}$  gauss), as found from other magnetic evolutions. With a toroidal field there is no reason to expect a continuum of modes, since this feature has only been established for fields with a poloidal component. Indeed, all our results have shown discrete mode frequencies, with no dependence on position within the star, up to uncertainties due to resolution and the

finite duration of our simulations (in practice, errors of  $\sim 1\%$ ). Our polar  $a$ -modes thus share this property with those of Sotani et al. (2008), but our axial  $a$ -modes are discrete too.

Purely toroidal fields and purely poloidal fields suffer from generic localised instabilities, so in the absence of damping mechanisms are not viable candidates for long-lived stellar magnetic fields (Wright 1973; Tayler 1973). Despite this, we have been able to perform stable evolutions of perturbations about a purely toroidal background for this work. There may be a number of reasons why these analytically-established instabilities have not affected our numerical work. Since we only consider first-order perturbations, higher-order effects are avoided; at the linear level, the greatest instabilities are those for  $m = 0$  and  $m = 1$ , whilst we have only considered  $m \geq 2$ . Finally, we have included artificial viscosity and resistivity to damp numerically-generated instabilities, and it is possible that these have prevented the growth of physical instabilities too.

One way in which pure-poloidal/toroidal fields may be stabilised is through rotation (Geppert & Rheinhardt 2006; Braithwaite 2006; Kiuchi et al. 2008), although this effect will be small in the case of the magnetars, whose rotational periods are very long. Relatively small poloidal components may stabilise dominantly toroidal fields (Braithwaite 2009), but it is difficult to draw general conclusions on the relative strengths of the two components, since other work (Lander & Jones 2009; Cioffi et al. 2009) has found that apparently general constructions of magnetic stars in equilibrium (in both Newtonian and relativistic contexts) result in mixed fields which are dominantly *poloidal*.

Given the many uncertainties regarding the nature of stellar magnetic fields, we believe that it is reasonable to study oscillations of purely toroidal fields, even though these may suffer certain instabilities, as we have discussed. Furthermore, a star whose field is dominantly toroidal could be expected to have an oscillation spectrum with similar features to those discussed in this paper.

The observations of QPOs in the tails of giant flares from magnetars may be providing a rare probe of the interior fields of these stars. In addition, the longer-term prospect of studying gravitational-wave signals from neutron stars using detectors like Advanced LIGO and VIRGO should also help understand the physics of these stars. With a clearer picture of the nature of stellar oscillations in a strong magnetic field, we should be better equipped to interpret magnetar QPOs and GW signals of neutron stars. Our formalism allows us to build up a more sophisticated picture of the oscillation spectrum of magnetised stars by a gradual inclusion of extra effects. These could include other field geometries, stratified stars, a superfluid interior, and so on; we intend to explore these in future work.

## ACKNOWLEDGMENTS

We thank Nils Andersson for useful discussions and advice. This work was supported by STFC through grant number PP/E001025/1 and by CompStar, a Research Networking Programme of the European Science Foundation.

## REFERENCES

- Andersson N., Kokkotas K.D., 2001, International Journal of Modern Physics D, 10, 381
- Brackbill J.U., Barnes D.C., 1980, J. Comp. Phys., 35, 426
- Braithwaite J., 2006, A&A, 453, 687
- Braithwaite J., 2009, MNRAS, 397, 763
- Cerdá-Durán P., Stergioulas N., Font J.A., 2009, MNRAS, 397, 1607
- Chandrasekhar S., Limber D.N., 1954, ApJ, 119, 10
- Cioffi R., Ferrari V., Gualtieri L., Pons J.A., 2009, MNRAS, 397, 913
- Colaiuda A., Beyer H., Kokkotas K.D., 2009, MNRAS, 396, 1441
- Cox J.P., 1980, Theory of Stellar Pulsation, Princeton University Press
- Dedner A., Kemm F., Kröner D., Munz C.-D., Schnitzer T., Wessenberg M., 2002, J. Comp. Phys., 175, 645
- Dziembowski W.A., Goode P.R., 1996, ApJ, 458, 338
- Friedman J.L., Schutz B.F., 1978, ApJ, 221, 937
- Gaertig E., Kokkotas K.D., 2009, PRD, 80, 064026
- Geppert U., Rheinhardt M., 2006, A&A, 456, 639
- Glampedakis K., Andersson N., 2007, MNRAS, 377, 630
- Goossens M., Poedts S., Hermans D., 1985, Solar Phys., 102, 51
- Israel G.L. et al., 2005, ApJ, 628, L53
- Jones D.I., Andersson N., Stergioulas N., 2002, MNRAS, 334, 933
- Kiuchi K., Shibata M., Yoshida S., 2008, PRD, 78, 024029
- Lander S.K., Jones D.I., 2009, MNRAS, 395, 2162
- Lee U., 2007, MNRAS, 374, 1015
- Ledoux P., Simon R., 1957, AnAp, 20, 185

- Levin Y., 2007, MNRAS, 377, 159  
Lockitch K.H., Friedman J.L., 1999, ApJ, 521, 764  
Morsink S.M., Rezanian V., 2002, ApJ, 574, 908  
Passamonti A., Haskell B., Andersson N., Jones D.I., Hawke I., 2009, MNRAS, 394, 730  
Price D.J., Monaghan J.J., 2005, MNRAS, 364, 384  
Rincon F., Rieutord M., 2003, A&A, 398, 663  
Sotani H., Kokkotas K.D., Stergioulas N., 2008, MNRAS, 385, L5  
Sotani H., Kokkotas K.D., 2009, MNRAS, 395, 1163  
Stergioulas N., Apostolatos T.A., Font J.A., 2004, MNRAS, 352, 1089  
Tayler R.J., 1973, MNRAS, 161, 365  
Unno W., Osaki Y., Ando H., Saio H., Shibahashi H., 1989, Nonradial Oscillations of Stars, University of Tokyo Press  
Watts A.L., Strohmayer T.E., 2007, Adv. Space Res., 40, 1446  
Wickramasinghe D.T., Ferrario L., 2000, PASP, 112, 873  
Wright G.A.E., 1973, MNRAS, 162, 339